



Numerical Investigation on the Effect of Dry and Wet Compression on a Linear Low Speed Compressor Cascade

D. Narayanan[†], S. Anand and S. Anish

Turbomachinery Laboratory, Mechanical Department, National Institute of Technology, Karnataka, 575025, India

[†]Corresponding Author Email: narayanandeepak10@gmail.com

(Received January 16, 2019; accepted May 25, 2019)

ABSTRACT

Several techniques are implemented to reduce the temperature rise in multistage compressors, which leads to the noticeable improvement in specific power output of a gas turbine. The objective of the present investigation intends to understand the effect of incidence angles on the aerodynamic performance of the compressor cascade under wet compression. Using large eddy simulations (LES) the effects of wet compression on compressor flow separation and wake formation are investigated. Experimental investigation was performed to validate the numerical results. The study reveals notable flow modifications in the separated flow region under the influence of wet compression and the total loss coefficient reduces significantly at the downstream side of the compressor for positive incidence angles. On the other hand, for negative incidence angles the wet compression enhances the total pressure losses inside the blade passage. Also, in the present investigation, particular emphasis has been given to understand the water film formation at negative and positive incidence angles.

Keywords: Wet compression; Large eddy simulation; Linear compressor cascade; Incidence angle; Flow loss.

NOMENCLATURE

C_{ax}	axial chord length	m_w	mass flow rate of water droplet at inlet
C_{po}	local total pressure loss coefficient	m_∞	mass flow rate of mainstream at inlet
$\overline{C_p}$	pitch averaged static pressure loss coefficient	P_s	static pressure
$\overline{\overline{C_{po}}}$	mass averaged total pressure loss coefficient	P_t	total pressure
i	incidence angle	$P_{t,w}$	total pressure of water droplets at inlet
		$P_{t,\infty}$	total pressure of mainstream at inlet
		U_∞	mainstream average inlet velocity

1. INTRODUCTION

Wet compression technique (also known as overspray) has been successfully employed in many gas turbines power generation industries due to their higher efficiency (Bhargava *et al.*, 2007; Jolly & Cloyd, 2003; Meher-Homji & Mee, 2000). An increase in the power output and heat rate of about 5.6% and 2% respectively were reported in Alstom GT24 with an overspray of 1.2% (Jolly & Cloyd, 2003). The advantages of using wet compression and the parameters that are causing changes in compressor and overall gas turbine performance

were detailed in many previous studies (Bhargava & Meher-Homji, 2002; Sexton & Sexton, 2003; Shao & Zheng, 2005; Zheng *et al.*, 2002; Zheng *et al.*, 2003). The specific compression work decreases due to wet compression was demonstrated with thermodynamic models by Zheng *et al.* (2002). Bhargava & Meher-Homji (2002) conducted parametric study of gas turbines with inlet evaporative and over spray fogging, and found that combination of fogging and overspray would produce more output for the same amount of water flow (Sexton & Sexton, 2003). Wet compression and regenerative (WCR) gas turbine is an economically

competitive option for efficient gas turbines (Zheng *et al.*, 2003). The stage stacking study on GE9E gas turbine revealed an increase in performance and efficiency of about 20% and 3% respectively with 1% water injection.

The physical mechanism of wet compression is too complex as there are too many parameters involved in the evaporation process. Unlike inlet fogging, the overspray demands the presence of water droplets within the blade passage. The physical mechanisms involved in these processes can be categorized as droplet-droplet, droplet-air and droplet-wall interactions. Droplet size has an effect on the irreversible entropy production, evaporation rate, compression outlet temperature and compressor specific work. Utamura *et al.* (1999) observed that water droplets with mean diameter 10 μm do not hit the rotor blades whereas 100 μm droplets are expected to hit it. During wet compression continuous evaporation takes place in the compression process which leads to reduction in compressor specific work (Horlock, 2001).

The water droplets get evaporated and this will lead to less loading on the front stages and overloading on the rear stages (Hartel & Pfeiffer, 2003). This was corroborated later by the study of White and Meacock (2003) on a 12-stage compressor. Unloading of earlier stages and increased loading at later stages were observed. Due to reduced aerodynamic efficiency and thermodynamic losses, the work reduction due to evaporative cooling was found less. Droplets with smaller value of Sauter Mean Diameter (SMD) would result in an increased evaporation rate (Bhargava *et al.*, 2007). In fact, the evaporation rate, unloading, and loading of earlier, and later stages of compressor were affected by the droplet size (Khan & Wang, 2009; Wang & Khan, 2008; Wang & Khan, 2008).

Several numerical works detailed more about the droplet air and droplet wall interactions (Khan & Wang 2008, Nikolaidis *et al.*, 2008; Payne & White, 2008; Williams & Young, 2006; Lin *et al.*, 2018). Smaller droplets (5 -10 μm) exhibits zero slip before entering the rotor passage. However, inside the blade passage slip velocity may be influenced by the local pressure gradient in the pitch wise direction. Studies conducted by Williams and Young (2006) showed that inertia and friction forces affect the droplet motion and the effect of aerodynamic shear force depends on the extend of film formation over the blade surface. The droplet trajectory is unlikely to be affected by the pressure gradient. The blade pressure distribution may be affected by the impact of the droplet on the blade surface (Payne & White, 2008). Studies carried out by Sun *et al.* (2008) showed that separated region on the rotor blades suction surface could be removed using wet compression. For analyzing the changes in the performance characteristics before and after water injection a comparative study has been conducted and which concluded that in low frequency region high performance fluctuation will be occurred due to the phase changes of the droplets (Lin *et al.*, 2019a).

To analyze two-phase flow combined with the

evaporation of water droplets a three-dimensional analysis method was developed by Payne and White (2008). The model applied to a single stage compressor with droplet size of 4 μm showed a decrease in axial velocity which results in a change in blades pressure distribution. Several researchers experimentally investigated the movement of water droplets after they fall into the rotor blade walls of a transonic compressor with wet compression (Eisfeld & Joos, 2009; Ulrichs & Joos, 2006). Experiments were conducted by Ulrichs and Joos (2006) with free stream conditions of Mach number 0.7 and droplet size having Sauter Mean Diameter of approximately 16-36 μm showed two behaviors of droplets. First, droplets below 10 μm are separated in the latter one-third part of suction surface and second, at the trailing edge a water film is formed which leads to ligament formation whereas, Sun *et al.* (2013) showed that water droplets smaller than 5 μm can achieve complete evaporation upstream of the combustor and bigger droplets have to enter into the combustor to achieve full evaporation. This shows that fine mists should be provided for water injection if full evaporation is needed before the combustor. Another experiment conducted by Eisfeld and Joos (2009) examined the floor phenomenon on a transonic compressor with free stream Mach number 0.85 and water injection ratio of 2%. The results showed that droplets when falls on the rotor blades leading edge turns into larger amount of small droplets due to splashing and this in turn affect the evaporation rate. Once the injected water droplets fall on the blade surface and form a water film, then it will shift to the rear of the upper half of the blade surface due to combined effect of centrifugal and aerodynamic shear force (Williams & Young, 2006).

The available literatures show that extensive research has been carried out to understand the interaction of the droplets with compressor blade. Most of the studies are focused on the droplet size and injection ratio. There is a scarcity of fundamental research into the effects of water injection at different incidence angles on the aerodynamic performance and stability of compressor blades. Hence in the present study, a numerical analysis has been carried out at constant injection ratio with fixed droplet diameter for different incidence angles, in order to understand the performance of a linear compressor cascade. The effects of water injection on the loss coefficient and formation of water film are particularly noted in the present study.

2. METHODOLOGY

A linear compressor cascade available at Turbomachinery Laboratory, NITK has been chosen for the present study. It is a low speed linear cascade and the blades are designed such that they have aerodynamic similarity to real machines rather than geometrical similarity. It operates at a Reynolds number several times lower than a real compressor. The wind tunnel is of blown down type with an axial flow fan. It consists of a circular entrance section

with a conical inlet containing a safety screen (Fig. 1). The fan is driven by 5kW AC motor (440V, 3-Phase) equipped with a variable frequency drive. Downstream of the fan is the settling chamber, consisting of screens and a straw honey comb. A water injection system is fitted downstream of the honeycomb with jet type nozzles to provide fine droplets. A 0.5 HP pump with a 50 cm×50 cm×80 cm tank is provided for water supply. A digital flow controller is provided to vary injection mass flow rate. Nozzle is dismantlable. Three nozzles are arranged inside settling chamber providing equal distance between nozzles. It is fitted to the root of the stem by making internal thread. The test section is bolted to the exit of a contraction section. The cascade pack is mounted on a horizontal circular base so that the complete base and the pack can be rotated on a vertical axis to set to the required inlet angle and it is supported by a table (Fig. 2). The possible range of incidence angles is ± 20 degrees from the center position of the variation mechanism. The maximum speed at the test section is 30 m/s. The test section (450 mm×120 mm) is equipped with five compressor blades, made of aluminum, in a linear cascade configuration mounted between two side walls. A minimum of five blades is kept in order to improve the periodicity of the flow. The side walls of the test section are made with acrylic glass. The test rig is equipped with a probe traversing mechanism to understand the flow modifications at the blade exit. A five hole probe is used to take the measurements at the downstream of the blade. Detailed specifications of the cascade are given in Table 1.



Fig. 1. Low speed compressor cascade wind tunnel.



Fig. 2. Test section showing compressor blades.

2.1 Geometrical Modeling and Meshing

For the numerical study a single compressor blade passage is modeled using ICEM CFD. The inlet of

the fluid domain is 1.5 times the axial chord distance (C_{ax}) upstream of the blade leading edge, whereas the outlet plane is kept at a distance of 1.25 times the axial chord distance downstream of the trailing edge. Entire span of the blade is modeled and along the transverse direction, translational periodicity is set at one pitch length. The computational domain is filled with structured grid elements. Near the blade surface and end walls fine mesh is provided with hexahedral layers to take care of the boundary layer effects. The first cell height normal to the surface is 0.0140 mm and the last cell height is 0.1285 mm. There are 70 layers in between, through which the cell height is increasing exponentially as shown in (Fig. 3).

Table 1 Details of linear compressor cascade

Number of blades	5
Test Section Size	450 mm×120 mm
Axial Chord	120 mm
Span	120 mm
Pitch to Chord ratio	112 mm
Inlet Metal Angle	47 deg.
Outlet Metal Angle	90 deg.

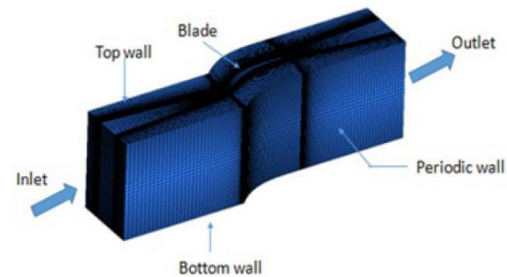


Fig. 3. Computational domain with structured grid elements used for the simulations.

2.2 Solver Details

For simulating the complex turbulent flows in the compressor cascade, an accurate turbulence model needs to be selected. In this study, unsteady RANS and LES models are tested. A time step of 5×10^{-6} s is given for all these simulations. Shear Stress Transport (SST) model is used in the case of RANS and Smagorinsky model is selected for LES. These are widely used and validated turbulence models with appliances ranging from industrial to environmental flows. The values of the total pressure and total temperature prescribed at compressor inlet are 220 Pa and 303 K respectively. Outlet boundary is defined with air mass flow rate of 0.157 kg/s. Boundary condition chosen for the periodic surface is conservative interface flux. No slip and adiabatic conditions are specified on the end walls and blade surface. For simulations with water injection, air is the continuous fluid and water droplets is set as the Lagrangian fluid. Water injection at the compressor inlet assumed to be uniform and the water diameter distribution follows the law of Rosin-Rammler which states that the mass fraction and droplet

diameter are related exponentially as in the Eq. (1)(Lin *et al.*, 2019b).

$$Y_d = \exp\left(-\left(\frac{d}{d_0}\right)^n\right) \quad (1)$$

where ' Y_d ' mass fraction of droplets, ' d ' is the size constant and ' n ' is size distribution parameter. Water injection system which is fitted with the Experiment test rig can provide an average water droplet size of 20 micron. Hence incorporating the experimental conditions in the numerical simulation the value of Rosin-Rammler size is kept 20 micron with exponential power value of 1.5. Droplets are specified as fully coupled to continuous fluid. Wall film formation due to the droplet interaction with the blade surface is considered for this study. Accordingly, Elsaesser model is chosen for the droplet wall interaction. Aluminum and steel are selected for blade and bottom end wall respectively. When the water droplets impact on the top wall, wall interaction is studied in terms of perpendicular and parallel coefficient of restitution. The given values are 0 and 1 respectively on the assumption that the particles which are bouncing due to the impingement on the top wall will be deposited on it after a period of time. Hence the particles that stick to the wall is having perpendicular coefficient value close to zero. Simulations are carried out by varying the incidence angles. Primarily six incidence angle has been considered other than the nominal incidence angle; these are -5 deg., -10 deg., -15 deg., +5 deg., +10 deg. and +15 deg. If the flow is leaning towards the pressure surface, it is regarded as a positive incidence (Fig. 4).

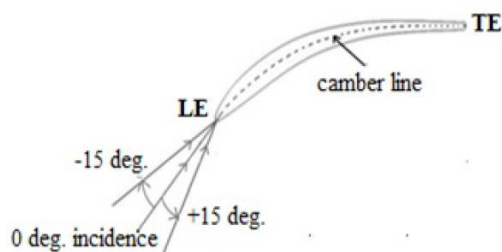


Fig. 4. 2D schematic representation of zero incidence, positive incidence and negative incidence.

2.3 Verification and Validation

Hexahedral elements were used in LES studies. However instead of using LES, the initial mesh independence study has been carried out using the shear stress transport (SST) transitional flow model for getting the advantage of reducing total computation time for the investigation. A very fine near wall resolution, with maximum y^+ value less than 2 has been achieved. Meshing has been carried out in such a manner that, approximately ten grid nodes are fitted inside the boundary layer, owing to the requirements of the low-Re turbulence model. The comparison between cases of various grid elements reveals that a difference of only 2% was obtained between the 2 million element mesh and a

finer mesh of 5 million elements (Fig. 5).

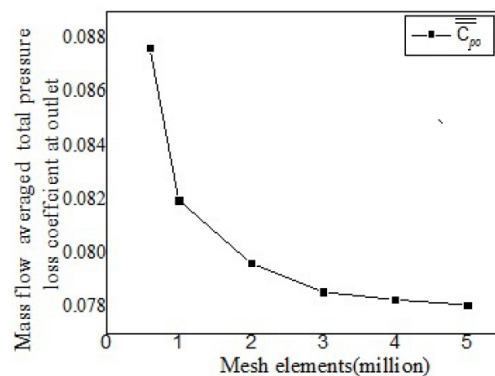


Fig. 5. Primary grid independent study with RANS .The variation of mass averaged total pressure loss coefficient ($\overline{C_{po}}$) is shown against various number of grid elements.

In the case of LES , the outcome will be much more precise if the mesh elements is being increased. On the other hand, Large eddy simulation (LES), resolves the larger turbulent eddies whereas the smaller ones are modeled. Computational cost of LES is comparatively higher than RANS. Very fine grids have been generated for LES so that the maximum value for y^+ can be maintained smaller than 1 and Δx^+ , ΔZ^+ values within 50 and 20 respectively (classically retained values) to capture near wall turbulent structures. 15 million point grid containing 636, 131 and 180 points in the stream wise, wall normal and span wise direction respectively has been chosen for this present study ($\Delta x^+ = 42$, $\Delta Z^+ = 15$). In LES, as the grids become finer the solution approaches to a Direct Numerical Simulation (DNS). The classic Smagorinsky LES model is closer to DNS data. Hence, the present simulation has been carried out with LES Smagorinsky model. In the present analysis, the upper limit for the number of elements is imposed by the limitations from the workstation.

Results obtained from LES are compared with experimental results. A five-hole probe is used for measuring the flow conditions at the downstream region of the blade. With help of probe traverse mechanism, measurements have been taken for every 1mm location along the pitch wise direction at different percentage of span. Total pressure loss coefficient (C_{po}) along non-dimensional pitch wise locations (x/s) are calculated and plotted for different span wise locations at 128.5% of chord distance. The C_{po} is calculated from the difference between the average inlet total pressure and the local total pressure at point of interest. This difference is then normalized with the inlet dynamic pressure.

Figure 6(a) and Fig. 6(b) shows the C_{po} comparison of experiment with LES along one blade pitch at 5%

and 10% span respectively. The models predict an increase in the losses at the wake region qualitatively. In addition to total pressure loss coefficient, wall static pressure coefficient on the end wall (top wall) are also validated with the experimental results. The test data is obtained from twelve rows of static pressure taps (each consisting of 7 holes) inside the blade passage and five rows of static pressure taps (each consisting 10 holes) at the downstream of the central blade on the top end wall (Fig. 7). Measured static pressures are then normalized with inlet dynamic pressure. The pressure coefficient obtained from the experimental investigation (Fig. 8(b)) exhibits almost same trend and nearly equal magnitude as that of computational results (Fig. 8(a)). In the case of water injection, the experimental investigations with intrusive probes are not feasible. Hence static pressure distribution at the end wall has been chosen for the validation of water injection study. From the plots (Fig. 9), it is visible that simulation results are matching with the experimental results qualitatively. The pitch averaged static pressure loss coefficient is determined in the case of water injection by the Eq. (2). When it is analyzed quantitatively, error is found to be within 11%. Maximum deviation is 10.

$$\overline{C_p} = \frac{\frac{m_\infty}{m_\infty + m_w} \overline{P_{s,\infty}} + \frac{m_w}{m_\infty + m_w} \overline{P_{s,w}} - \overline{P_s}}{0.5\rho_\infty U_\infty^2} \quad (2)$$

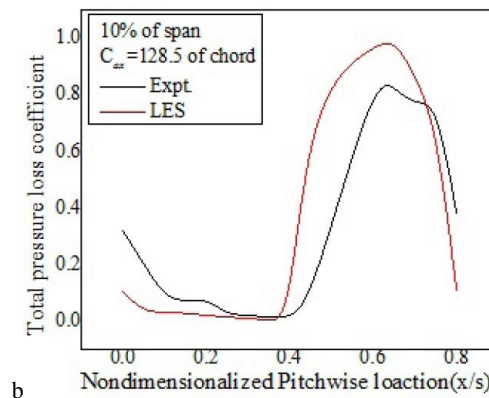
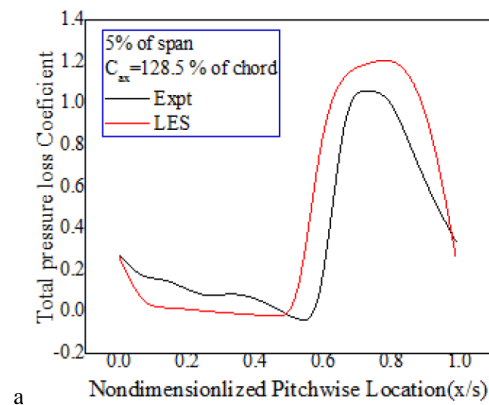
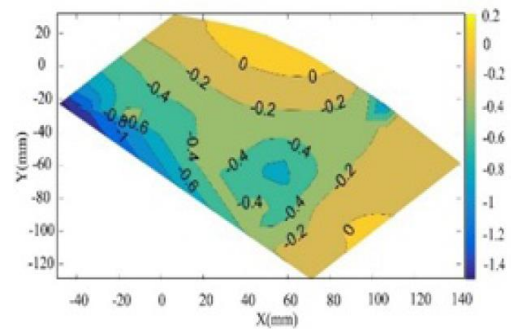


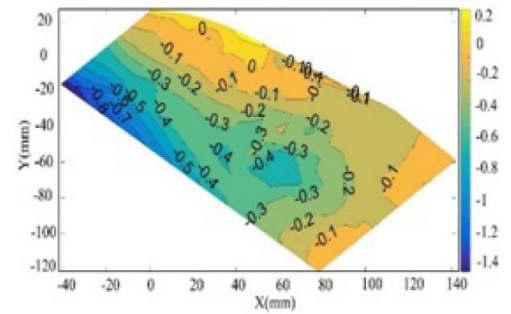
Fig. 6. Variation of total pressure loss coefficient along pitch wise direction for dry case (a) 5% span (b) 10% span.



Fig. 7. Static pressure tapping arrangement on the top end wall.



a



b

Fig. 8. Contour of static pressure coefficient on the top end wall for dry case (a) CFD (b) Experiment.

3. RESULTS AND DISCUSSIONS

3.1 Effect of Water Injection on Total Pressure Loss Coefficient at Different Incidence Angles

Mass averaged total pressure loss coefficient C_{po} at different axial chord locations from leading edge to 120% C_{ax} for different incidence angles are calculated and are plotted for dry air simulations where droplet injection is not considered (Fig. 10). The loss coefficients are increasing with the positive incidence (flow leaning towards the pressure surface), evidently due to the increased flow separation from the suction side of the blade. The mass flow averaged total pressure loss coefficient is maximum at +15 deg. incidence and minimum at -15 deg. incidence. The loss coefficient values are

smaller at increased negative incidences. The extreme positive angle +15 deg. constitutes the most highly loaded, higher flow-turning configuration. At these conditions, the cross-passage gradient establishes a strong secondary flow field, which transports the low-momentum boundary layer, flows to the suction side of the blade. The aerodynamic blockage associated with low momentum region is vulnerable to rapid growth in the negative stream wise pressure gradient and may ultimately lead to the flow separation. It is found that the losses are smaller at lower positive and higher negative incidence angles. The present study focuses on the effect of water injection on the separated flow region. An injection ratio (IR) of 1% is chosen for this study (IR= mass flow rate of air/mass flow rate of water droplet). Rosin-Rammler size of 20 micron with power of 1.5 have been injected at the inlet of the computational domain and simulations are carried out. Figure 11 shows the comparison of mass flow averaged total pressure loss coefficients for dry and wet cases. The definition of mass flow averaged total pressure loss coefficient accounting in the case of water injection is given by the Eq. (3)

$$C_{po} = \frac{\frac{m_\infty}{m_\infty + m_w} \overline{P_{t,\infty}} + \frac{m_w}{m_\infty + m_w} \overline{P_{t,w}} - \overline{P_t}}{0.5\rho_\infty U_\infty^2} \quad (3)$$

It is found that the losses in the total pressure can be regained by the upstream water injection for positive incidence angles. After 80% of chord, 30% reduction in pressure loss is achieved. The interaction between water droplets and air, enables the momentum and energy transfer to the separated flow regions. Due to this, velocity in the non-separated region for the wet case becomes higher (Fig. 12). As a result the total pressure reduction in the dry case is minimized by the water injection. It reflects in the total pressure loss coefficient. Hence it can be stated that the total pressure losses at higher positive incidence angles will be minimized by the water injection. Contrary to this, at negative incidence angles (Fig. 11) the losses are enhanced with water injection and the reasons are explained in the subsequent sections.

3.2 Effect of Water Injection on Flow Separation

Velocity contour superimposed with surface streamlines were plotted for +15 deg. incidence angle at 50% span for both dry and wet cases (Fig. 13 - Fig. 14) respectively. The disturbances are high in the flow passage as well as in the downstream region, particularly near the trailing edge for dry case. The separated flow region causes significant blockage in the blade passage. With the injection of water droplets, the blockage in the blade passage is brought down (Fig. 14). However, the circumferential mixing of the fluid streams from pressure surface and suction surface are diminished at the downstream side after the trailing edge. This establishes one favorable and another unfavorable outcome at the downstream side. The lower circumferential mixing accounts for a smaller mixing loss in the downstream region, which results in smaller total pressure loss coefficient. The

unpropitious outcome of the weaker mixing is that it results in a higher circumferential non uniformity at exit. Hence it can be concluded that the point of separation and the separated flow regions within the blade passage are almost similar in both wet and dry cases, but the mixing at the downstream side of the blade is affected by the presence of water droplets. Figure 15(a) and Fig. 15(b) show the total pressure contours at different stream wise planes for both dry and wet cases at -15 deg. incidence angle. The comparison between the dry case and wet case indicates major reduction in the total pressure which starts within the blade passage itself for the wet case. In wet case the fluid stream comes from the pressure surface side has smaller momentum, the loss core region at the downstream side seems to expand in the transverse direction (Fig. 15(b)). These contours suggest that the injection of water droplets weakens the mean stream flow inside the blade passage at high negative incidence angles.

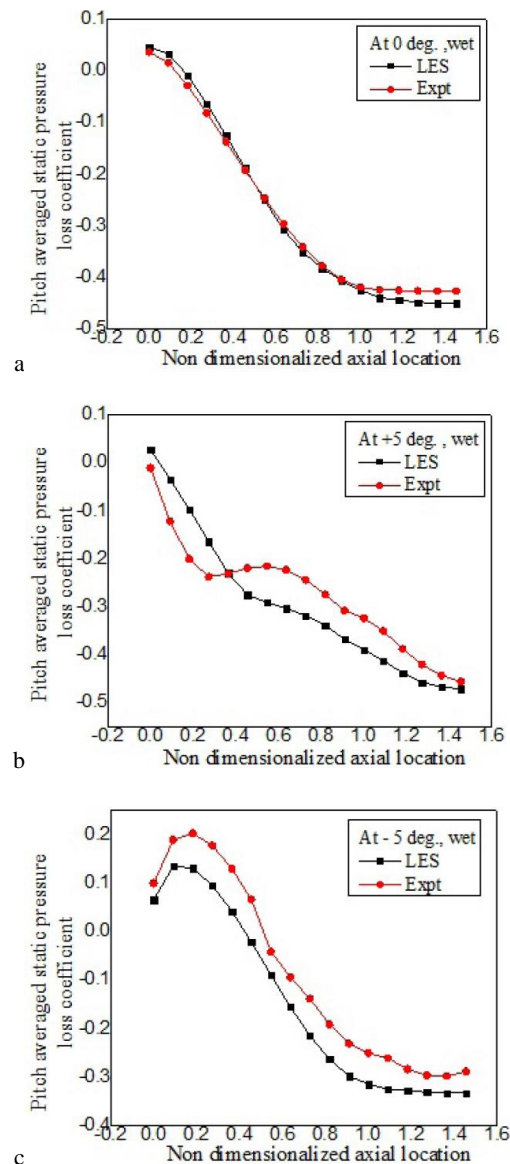


Fig. 9. Pitch averaged static pressure co-efficient on the top end wall (wet case) for different incidence angles (a) 0 deg. (b) +5 deg. (c) -5 deg.

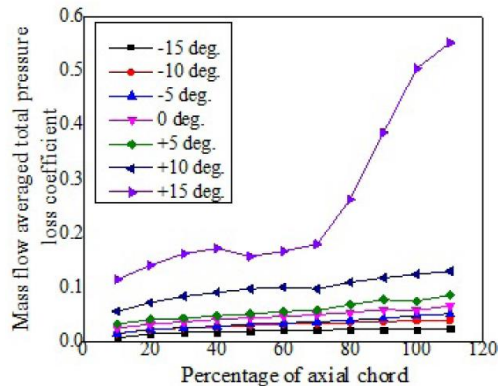


Fig. 10. Mass flow averaged total pressure loss coefficient at different incidence angles for dry air.

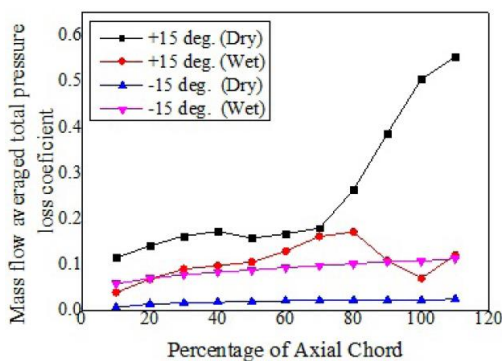


Fig. 11. Mass flow averaged total pressure loss coefficient for both Dry and Wet case at +15 deg. and -15 deg. incidence angles.

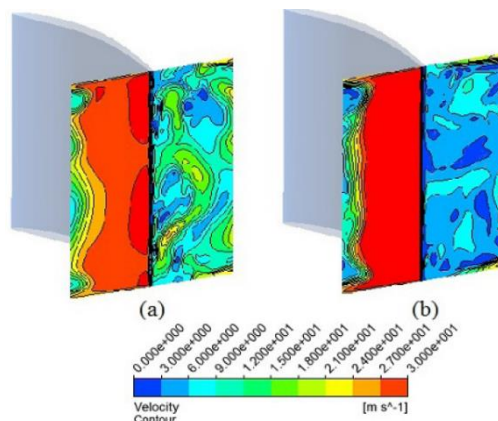


Fig. 12. Velocity contour at stream wise location near the trailing edge for (a) Dry and (b) Wet case at +15 deg. incidence angle.

3.3 Effects of Water Injection on Blade Loading

An analysis of the static pressure gradient in the transverse direction reveals a larger gradient on the wet case, particularly after the mid-chord region (Fig. 16). This pushes the separated flow region more towards the suction side, reducing the blockage. Near the trailing edge, pressure contour is found to be non-uniform for the wet case. The disturbances are high particularly in the separated flow regime. However,

these disturbances are not strong enough to affect the total blade loading as can be seen from the Fig. 17. Local undulations have been observed on the static pressure distribution on the suction surface of the blade. Similar results have been observed for other incidence angles also, hence not detailed here.

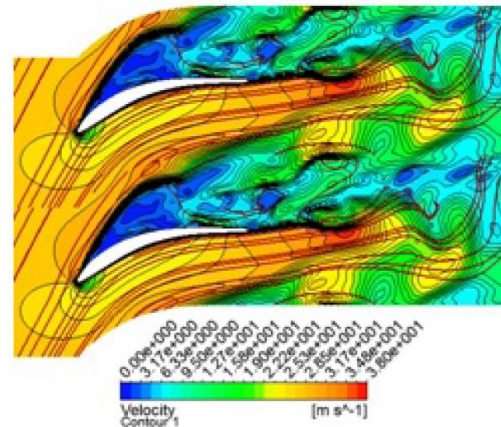


Fig. 13. Velocity contour superimposed with surface streamlines of dry case for +15 deg. incidence angle at 50% of span.

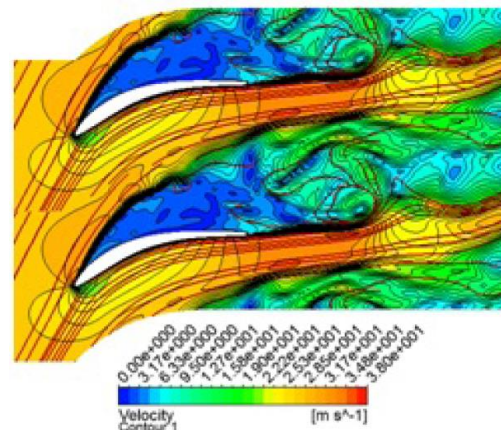
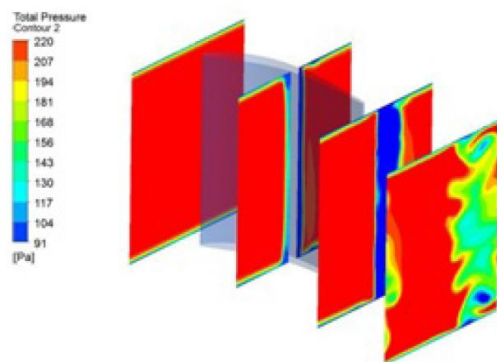


Fig. 14. Velocity contour superimposed with surface streamlines of wet case for +15 deg. incidence angle at 50% of span.

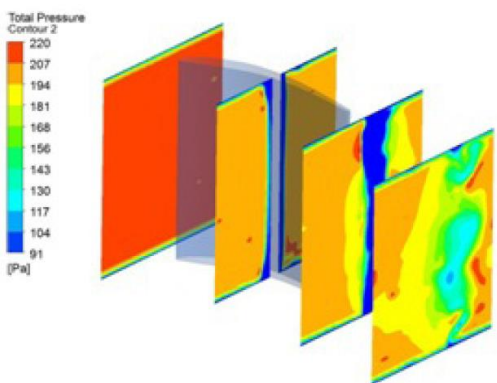
3.4 Formation of Wall Film Thickness

The effect of incidence angle on water film formation has been investigated and is discussed in this section. The analysis have been carried out at the same time step for all the incidence angles. This ensures the comparison is more meaningful. Water film formation is found to be more at the pressure surface for all the incidence angles. The thickness of water film formed over the blade surface is higher at small incidence angles and it is true for both positive and negative incidences. Figures 18 - 19 shows the contours of film thickness on the pressure surface of the blade at different incidence angles. The wall film is thicker after the midchord region for +5 deg. incidence angle, but it is thicker before the mid chord region at +15 deg. incidence. At negative incidence

angles, the film thickness is smaller at the pressure surface and almost negligible at -15 deg. incidence. The film formation largely depends on the droplet trajectories near the blade surface. At +5deg. incidence angle the droplets hits on the pressure surface at higher inclination to the surface near the leading edge region. In other words, a higher impact angle diminishes the chances of film formation. Impact angle (θ) may be defined as the acute angle formed by the tangent to the surface and the tangent to the trajectory. Figure 20 shows the impact angle at different axial chord location. Due to the curvature of the blade, the impact angle gets smaller at the mid chord region for +5deg. incidence angle. As a result, the wall film gets thicker in this region. At +15 deg. incidence angle the droplet trajectory is almost parallel to the blade near leading edge region on the pressure surface which result in a thicker film. On the other hand, after the leading edge a large impact angle is observed leading to a thinner film near mid-chord region and trailing edge region. Similar observations can be made with -5 deg. incidence angles also. However, at -15 deg. incidence angle the droplet trajectories hardly touches the pressure surface. As a result, the film formation is also minimum in this case.



a



b

Fig. 15. Total pressure contour inside the blade passage for -15 deg. (a) Dry case (b) Wet case.

It can be explained in detail by comparing the case of higher incidence angle +15 deg. and lower incidence angle +5 deg. For this analysis impact

angle has been measured in this cases at these regions (Fig. 21). Impact angle is found to be maximum near leading edge for both these cases and for +15 deg. incidence angle impact angle is reduced near the trailing edge. At +5 deg. incidence angle, the impact angle is not significantly varied at the mid-chord region. Maximum angles can be seen near leading edge region as well as the trailing edge region; in between, the impact angle is comparatively low. In both these cases, it can be observed that water film thickness is concentrated more near the region where impact angle is smaller whereas film formation is lower where impact angle is high. For -15 deg. incidence angle the formation of film thickness is smaller compared to other incidence angles.

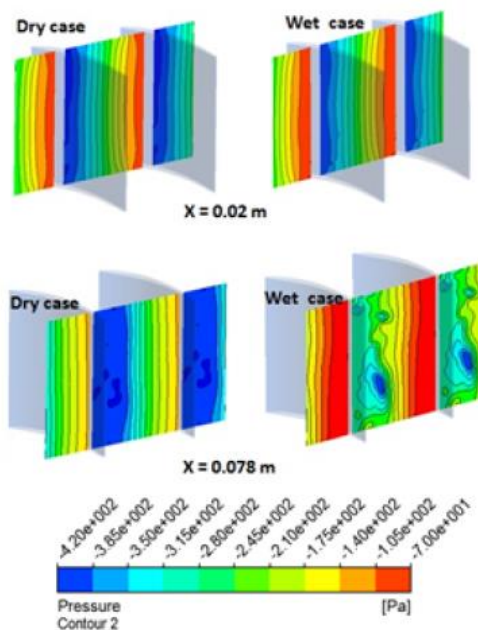


Fig. 16. Static pressure gradient within the blade passage; $i = +5$ deg. (X stands for distance from the leading edge).

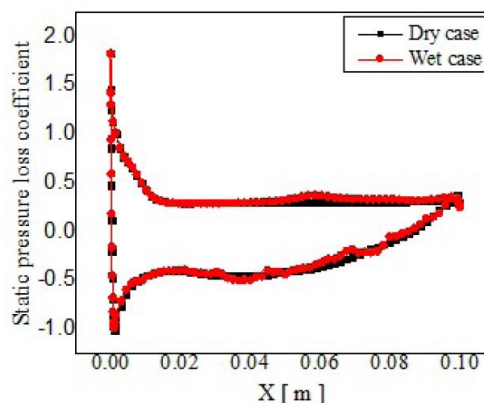


Fig. 17. Blade loading at +5 deg. incidence angle (X stands for distance from the leading edge).

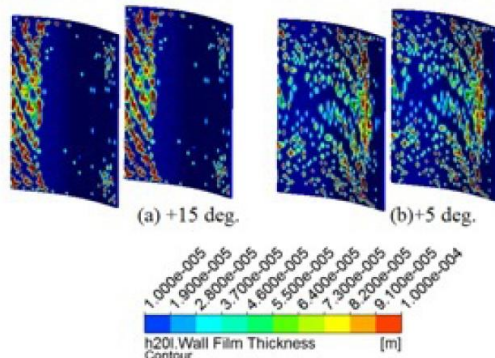


Fig. 18. Variation in water film thickness formation on pressure surface at (a) +15 deg. incidence angle and (b) +5 deg. incidence angle.

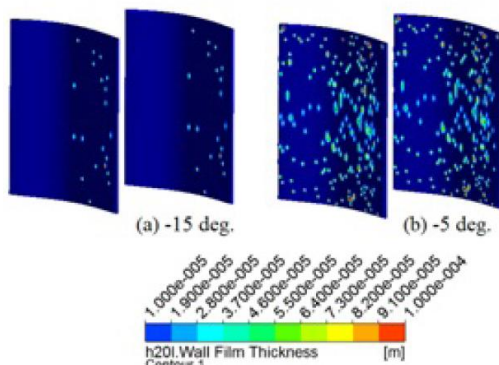


Fig. 19. Variation in water film thickness formation on pressure surface at (a) -15 deg. incidence angle and (b) -5 deg. incidence angle.

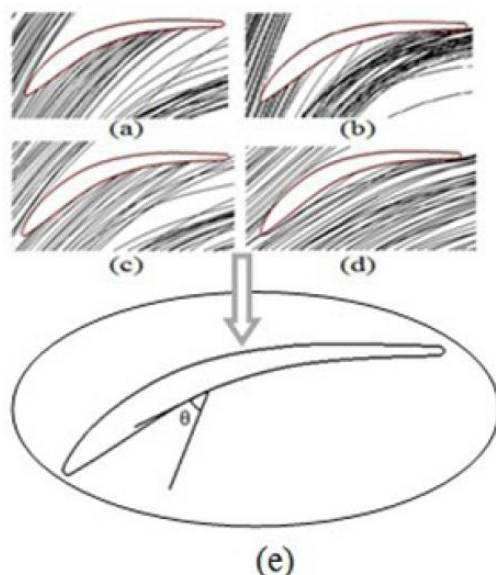


Fig. 20. Water droplets track on the computational domain at different angle (a) +5 deg., (b) +15 deg., (c) -5 deg., (d) -15 deg. and (e) schematic representation of impact angle(θ).

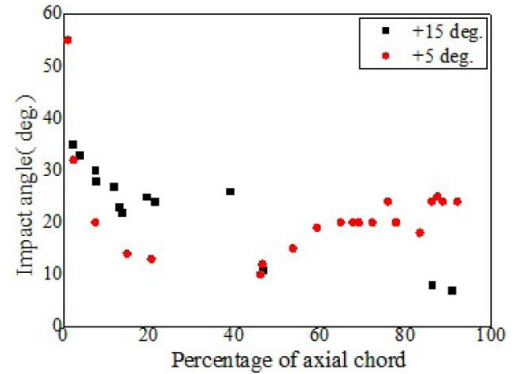


Fig. 21. Variation of impact angle along axial location for both +15 deg. and +5 deg. incidence angle.

3. CONCLUSIONS

A computational investigation is carried out to understand the effect of water injection on the separated flow regions in a compressor cascade at different incidence angles. The major findings of this investigation are detailed below.

The water injection produces two contrasting results at positive and negative incidence angles. With increase in the positive incidence angles water injection helps to reduce the loss coefficients inside the blade passage by controlling the separated flow regions, whereas for negative incidence angles, presence of water droplets enhances the loss generation inside the blade passage. It is also observed that the mixing of the jet and wake fluid streams at the downstream of the blade is diminished with the water injection.

The overall blade loading is not significantly affected by the droplet-wall interactions. However it may not be considered as a general recommendation. As the present investigation has been under taken on low speed compressor cascade, blade loading could be different on a subsonic or higher cascades. However small perturbations are observed on the suction surface of the blade. As a result, the pressure gradient in the transverse direction is affected. The wall film formation on the blade surface is varied at different incidence angles due to the variation in the particle trajectories. It is observed that, a smaller impact angle of the droplets on the blade surface tend to produce a thicker film.

ACKNOWLEDGMENT

The authors gratefully acknowledge the technical support by National Institute of Technology Karnataka (NITK) and financial support by Department of Science and Technology (DST), Ministry of human resource development.

REFERENCES

- Bhargava, R. and C. Meher-Homji (2002). Parametric analysis of existing gas turbines

- with inlet evaporative and overspray fogging. In *ASME Turbo Expo 2002: Power for Land, Sea, and Air*, 387–401. American Society of Mechanical Engineers.
- Bhargava, R., C. Meher-Homji, M. Chaker, M. Bianchi, F. Melino, A. Peretto and S. Ingistov (2007). Gas turbine fogging technology: A state-of-the-art review—part ii: Overspray fogging—analytical and experimental aspects. *Journal of engineering for gas turbines and power* 129(2), 454-460.
- Eisfeld, T. and F. Joos (2009). Experimental investigation of two-phase flow phenomena in transonic compressor cascades. In *ASME Turbo Expo 2009: Power for Land, Sea, and Air*, 103–112. American Society of Mechanical Engineers.
- Hartel, C. and P. Pfeiffer (2003). Model analysis of high-fogging effects on the work of compression. In *ASME Turbo Expo 2003, collocated with the 2003 International Joint Power Generation Conference*, pp. 689–698. American Society of Mechanical Engineers.
- Horlock, J. (2001). Compressor performance with water injection. In *ASME Turbo Expo 2001: Power for Land, Sea, and Air*, V001T03A039–V001T03A039. American Society of Mechanical Engineers.
- Jolly, S. and S. Cloyd (2003). *Performance enhancement of gt 24 with wet compression*. Power-Gen International, Las Vegas, NV, December, 9–11.
- Khan, J. R. and T. Wang (2008). Simulation of inlet fogging and wet-compression in a single stage compressor including erosion analysis. In *ASME Turbo Expo 2008: Power for Land, Sea, and Air*, 193–206. American Society of Mechanical Engineers.
- Khan, J. R. and T. Wang (2009). Overspray fog cooling in compressor using stage-stacking scheme with non-equilibrium heat transfer model for droplet evaporation. In *ASME Turbo Expo 2009: Power for Land, Sea, and Air*, 609–622. American Society of Mechanical Engineers.
- Lin, A., Y. Sun, H. Zhang, X. Lin, L. Yang and Q. Zheng (2018). Fluctuating characteristics of air-mist mixture flow with conjugate wall-film motion in a compressor of gas turbine. *Applied Thermal Engineering* 142, 779–792.
- Lin, A., Q. Zheng, Y. Jiang, X. Lin and H. Zhang (2019a). Sensitivity of air/mist non-equilibrium phase transition cooling to transient characteristics in a compressor of gas turbine. *International Journal of Heat and Mass Transfer* 137, 882–894.
- Lin, A., J. Zhou, H. Fawzy, H. Zhang, and Q. Zheng (2019b). Evaluation of mass injection cooling on flow and heat transfer characteristics for high-temperature inlet air in a mipcc engine. *International Journal of Heat and Mass Transfer* 135, 620–630.
- Meher-Homji, C. B. and T. R. Mee (2000). Inlet fogging of gas turbine engines: Part a—theory, psychrometrics and fog generation. In *ASME Turbo Expo 2000: Power for Land, Sea, and Air*, V003T03A008–V003T03A008. American Society of Mechanical Engineers.
- Nikolaidis, T., P. Pilidis, J. Teixeira, and V. Pachidis (2008). Water film formation on an axial flow compressor rotor blade. In *ASME Turbo Expo 2008: Power for Land, Sea, and Air*, 79–87. American Society of Mechanical Engineers.
- Payne, R. and A. White (2008). Three-dimensional calculations of evaporative flow in compressor blade rows. *Journal of Engineering for Gas Turbines and Power* 130(3), 032001.
- Sexton, W. R. and M. R. Sexton (2003). The effects of wet compression on gas turbine engine operating performance. In *ASME Turbo Expo 2003, collocated with the 2003 International Joint Power Generation Conference*, 673–679. American Society of Mechanical Engineers.
- Shao, Y. and Q. Zheng (2005). The entropy and exergy analyses of wet compression gas turbine. In *ASME Turbo Expo 2005: Power for Land, Sea, and Air*, 161–168. American Society of Mechanical Engineers.
- Sun, L., Y. Li, Q. Zheng and R. Bhargava (2008). The effects of wet compression on the separated flow in a compressor stage. In *ASME Turbo Expo 2008: Power for Land, Sea, and Air*, 219–236. American Society of Mechanical Engineers.
- Sun, L., Q. Zheng, Y. Li, M. Luo and R. K. Bhargava (2013). Numerical simulation of a complete gas turbine engine with wet compression. *Journal of Engineering for Gas Turbines and Power* 135(1), 012002.
- Ulrichs, E. and F. Joos (2006). Experimental investigations of the influence of water droplets in compressor cascades. In *ASME Turbo Expo 2006: Power for Land, Sea, and Air*, 221–230. American Society of Mechanical Engineers.
- Utamura, M., T. Kuwahara, H. Murata and N. Horii (1999). *Effects of intensive evaporative cooling on performance characteristics of land-based gas turbine*. Technical report, Hitachi Ltd.(JP).
- Wang, T. and J. R. Khan (2008). Overspray and interstage fog cooling in compressor using stage-stacking scheme: Part 1—development of theory and algorithm. In *ASME Turbo Expo 2008: Power for Land, Sea, and Air*, 99–109. American Society of Mechanical Engineers.
- White, A. and A. Meacock (2003). An evaluation of the effects of water injection on compressor

- performance. In *ASME Turbo Expo 2003, collocated with the 2003 International Joint Power Generation Conference*, 181–189. American Society of Mechanical Engineers.
- Williams, J. and J. B. Young (2006). Movement of deposited water on turbomachinery rotor blade surfaces. In *ASME Turbo Expo 2006: Power for Land, Sea, and Air*, 1407–1420. American Society of Mechanical Engineers.
- Zheng, Q., M. Li and Y. Sun (2003). Thermodynamic performance of wet compression and regenerative (wcr) gas turbine. In *ASME Turbo Expo 2003, collocated with the 2003 International Joint Power Generation Conference*, 813–820. American Society of Mechanical Engineers.
- Zheng, Q., Y. Sun, S. Li and Y. Wang (2002). Thermodynamic analyses of wet compression process in the compressor of gas turbine. In *ASME Turbo Expo 2002: Power for Land, Sea, and Air*, 487–496. American Society of Mechanical Engineers.